Supporting information

Reliable Lateral Zn Deposition Along (002) Plane by Oxidized PAN Separator for Zinc-Ion Batteries

Lei Luo[a], Zhaorui Wen[a], Guo Hong[b*], Shi Chen[a*]

[a.] Institute of Applied Physics and Materials Engineering, University of Macau, Avenida da Universidade, Taipa, Macau SAR, 999078 China.

[b.] Department of Materials Science and Engineering & Center of Super-Diamond and Advanced Films, City University of Hong Kong, 83 Tat Chee Avenue, Kowloon, Hong Kong SAR 999077, China.

*Corresponding authors:

Email: guohong@cityu.edu.hk (G. Hong), shichen@um.edu.mo (S. Chen)

1. Calculation Formula

(1) The electrolyte uptake = $\frac{W_S - W_O}{W_o} \times 100\%$

where W_O and W_S are the weights of the separator before and after it was soaked in the 2 M $ZnSO_4$ electrolyte, respectively.

(2) Calculation of ionic conductivity: To build the cell, the two stainless steel electrodes were separated by the OPAN and GF soaked with 2 M $ZnSO_4$ electrolyte. To achieve the resistance value, the EIS of the stainless steel/stainless steel cell was tested. Finally, the ionic conductivity (σ) is calculated using the equation:

$$\sigma = \frac{L}{R \times S}$$

Where L, R and S are the thickness of different separators, the resistance, and effective area.

(3) Calculation of ion transference number: To measure the ion transference number (τ), symmetric cells with different separators were assembled. The τ was determined using the CA and EIS tests, as well as the following formula:

$$\tau = \frac{I_s(\Delta V - I_O R_O)}{I_O(\Delta V - I_S R_S)}$$

Where the I_O and I_S are the initial and steady-state currents in the CA test, respectively. ΔV is the constant potential (25 mV). R_O and R_S are the interface impedances before and after the CA test, respectively.

2. Supporting Figures

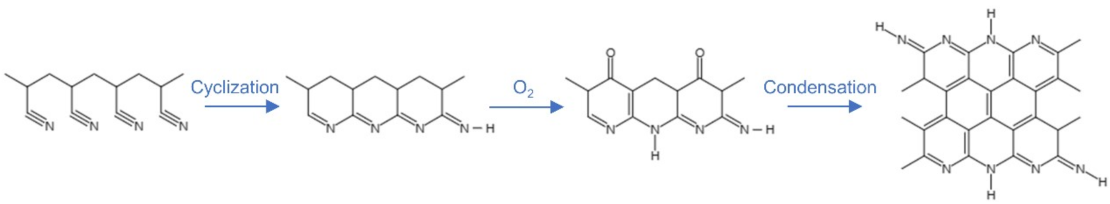

Figure S1 Scheme of conjugate planar structure generated by oxygen-induced intermolecular dehydrogenation reaction.

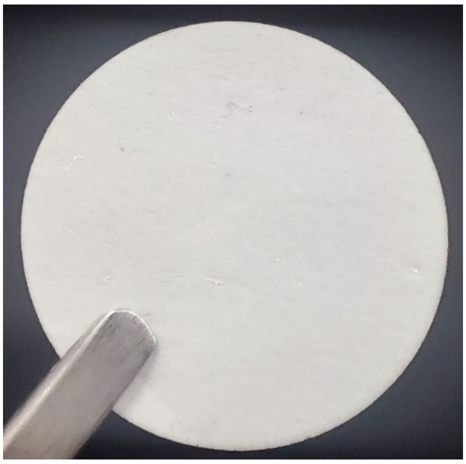

Figure S2 Optical photograph of PAN membrane.

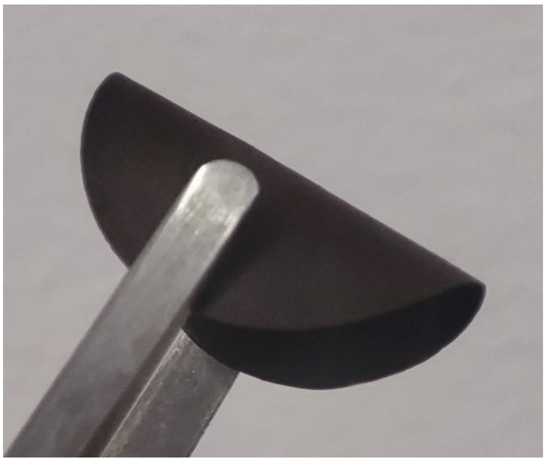

Figure S3 The flexibility of OPAN membrane.

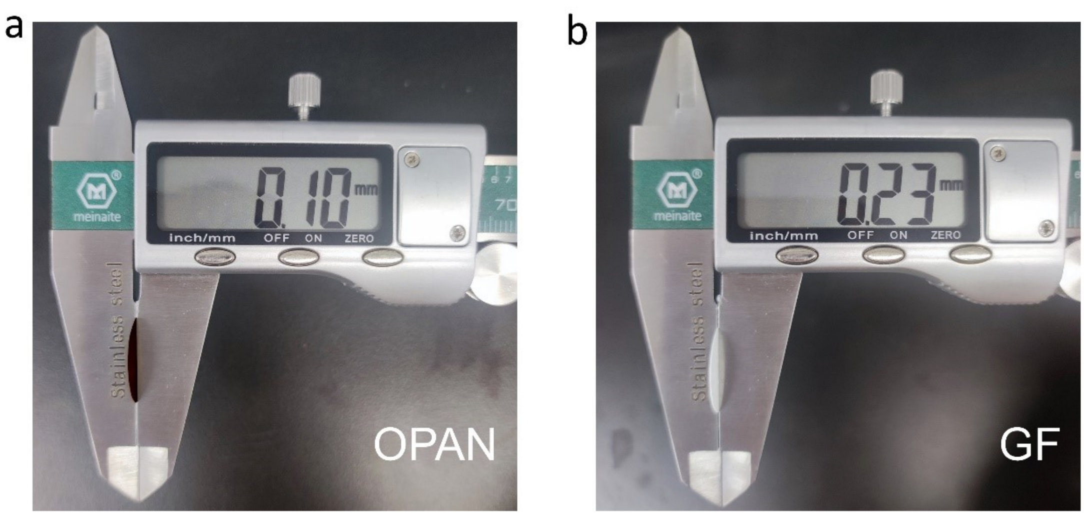

Figure S4 The thickness of OPAN and GF membranes.

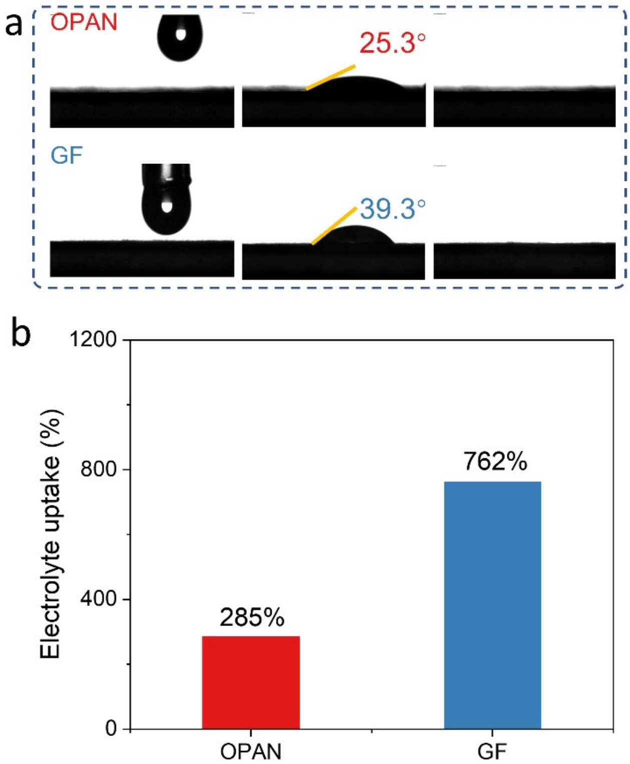

Figure S5 The water contact angles (a) and the electrolyte uptake (b) of OPAN and GF membranes.

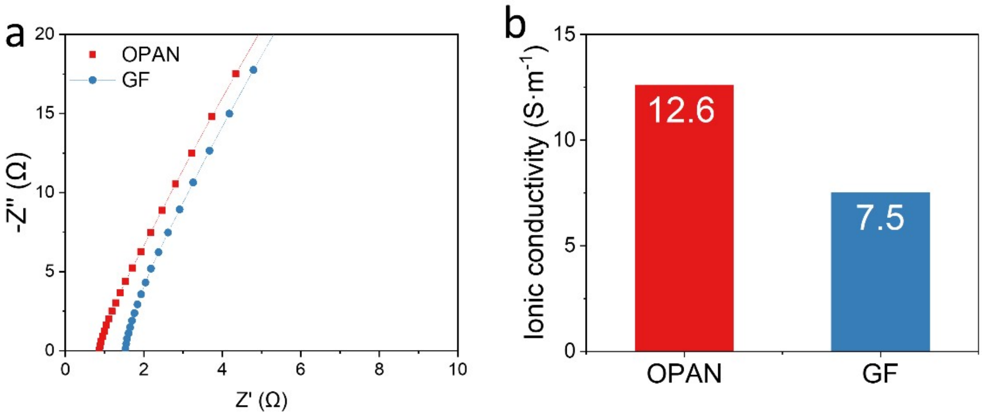

Figure S6 (a) EIS curves of stainless/OPAN/stainless cell and stainless/GF/stainless cell; (b) corresponding ionic conductivities of OPAN and GF.

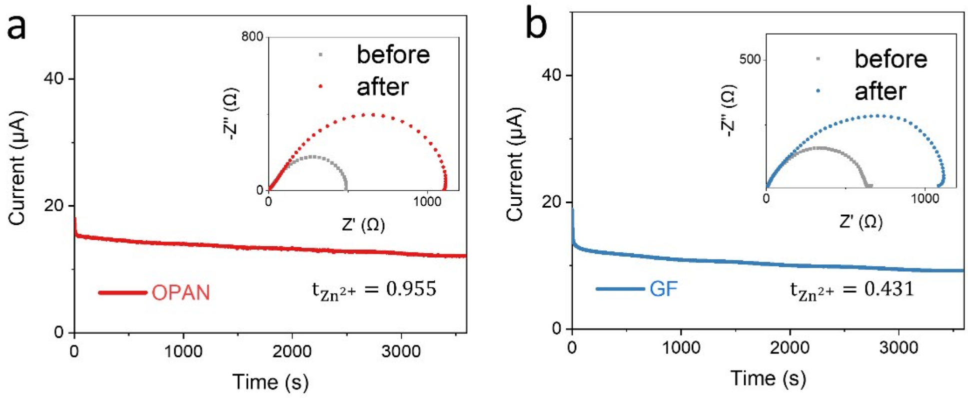

Figure S7 I–t curves of OPAN (a) and GF (b) at 25 mV potential and their corresponding EIS spectra before and after polarization.

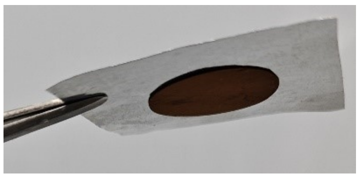

Figure S8 Electrostatic interaction of OPAN separator and Zn.

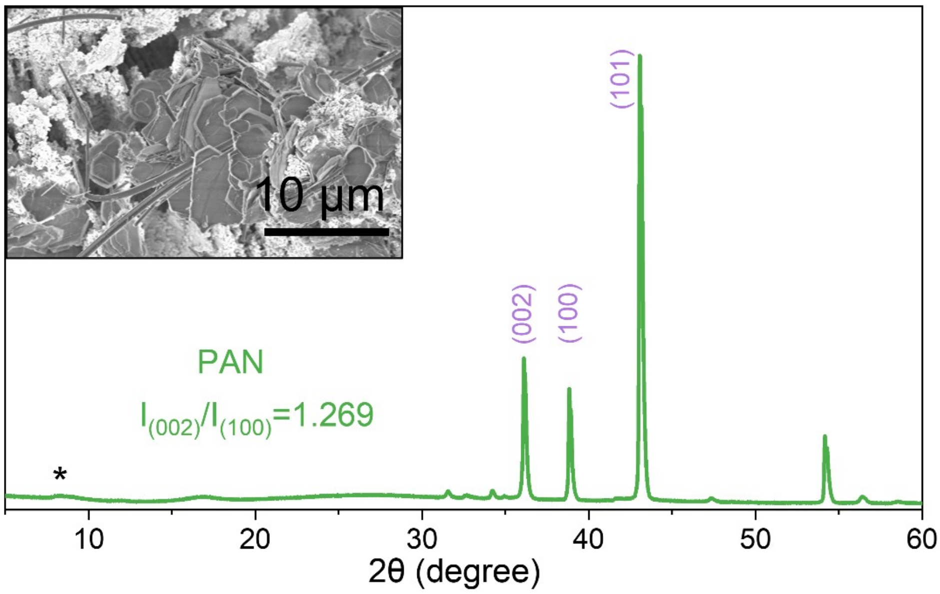

Figure S9 The XRD pattern of Zn anode after cycling using PAN separator.

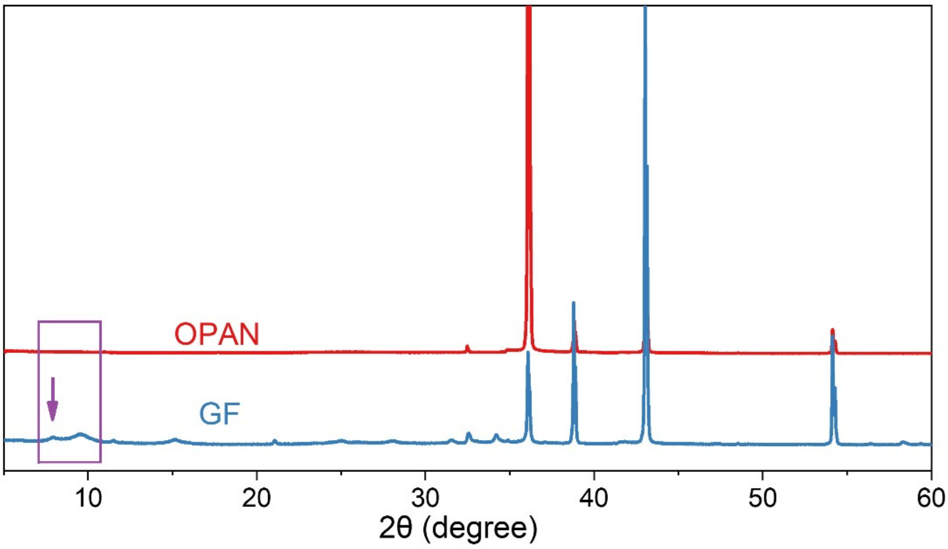

Figure S10 The XRD pattern of Zn anode after cycling using OPAN and GF separator.

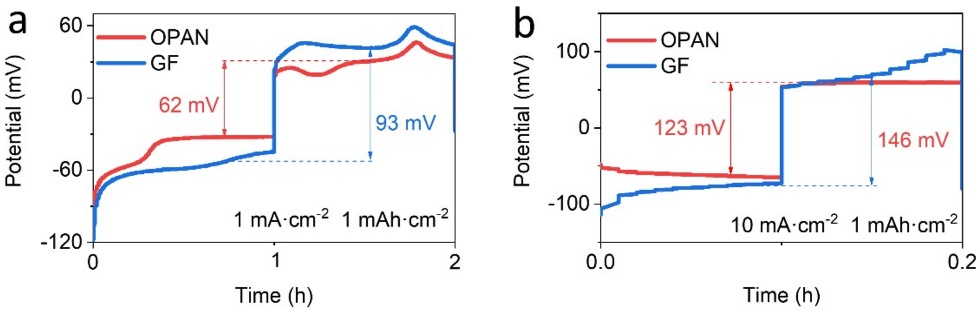

Figure S11 Polarization voltage of Zn symmetric batteries with OPAN and GF separators at current densities of (a) 1 mA·cm^{-2} and (b) 10 mA·cm^{-2}.

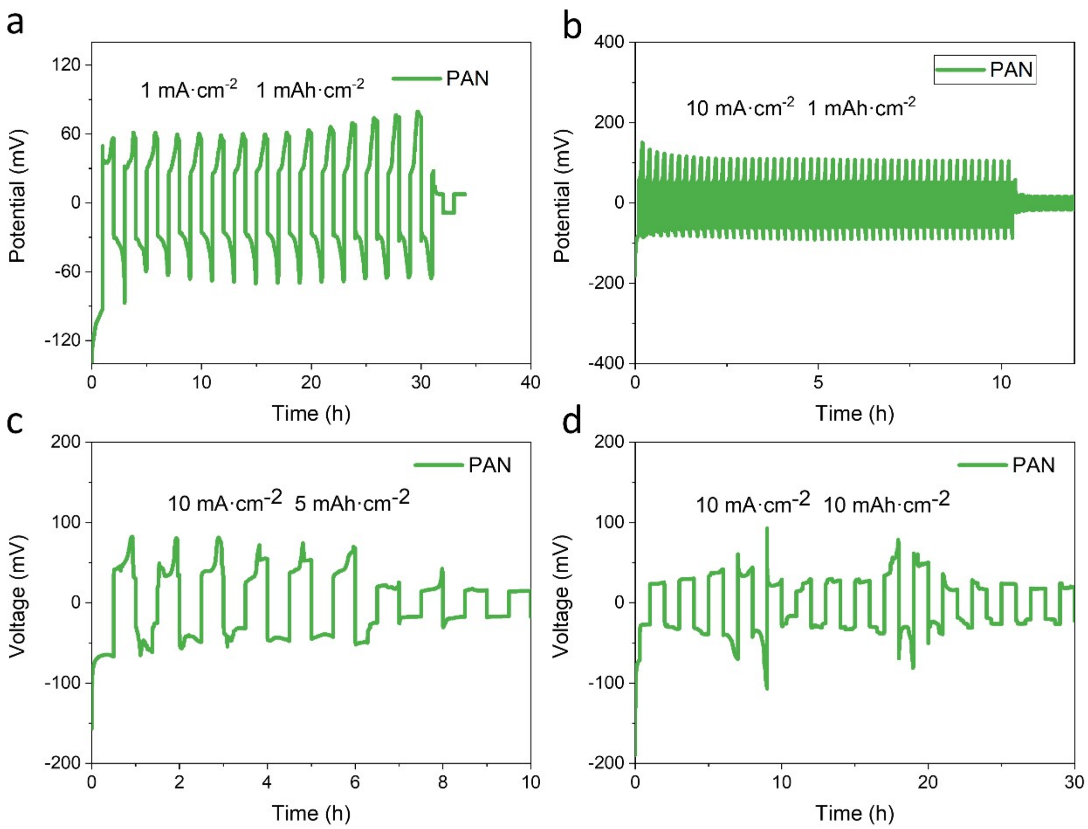

Figure S12 Cycling stability of Zn symmetric batteries with PAN separator at (a) 1 $mA\cdot cm^{-2}$, 1 $mAh\cdot cm^{-2}$; (b) 10 $mA\cdot cm^{-2}$, 1 $mAh\cdot cm^{-2}$; (c) 10 $mA\cdot cm^{-2}$, 5 $mAh\cdot cm^{-2}$; (d) 10 $mA\cdot cm^{-2}$, 10 $mAh\cdot cm^{-2}$.

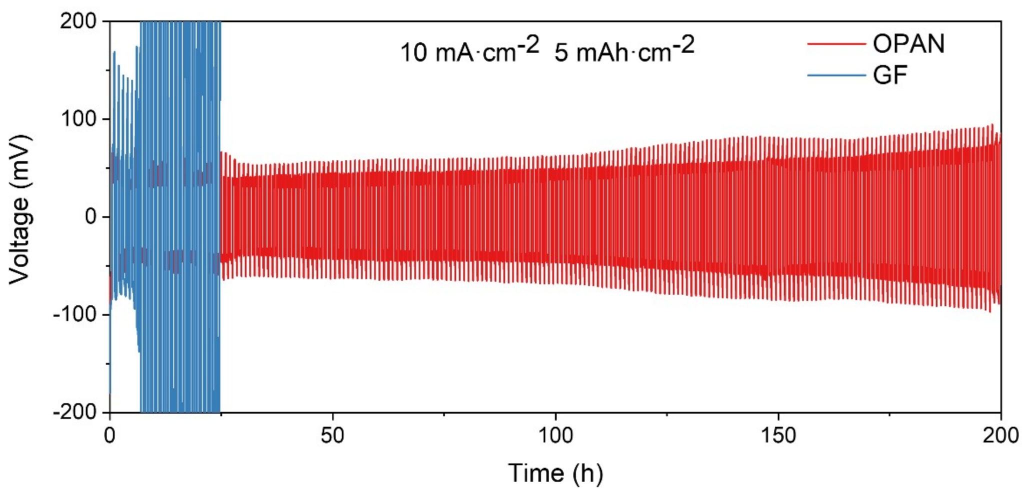

Figure S13 Cycling stability of Zn symmetric batteries with OPAN and GF separators at 10 mA·cm^{-2}, 5 mAh·cm^{-2}.

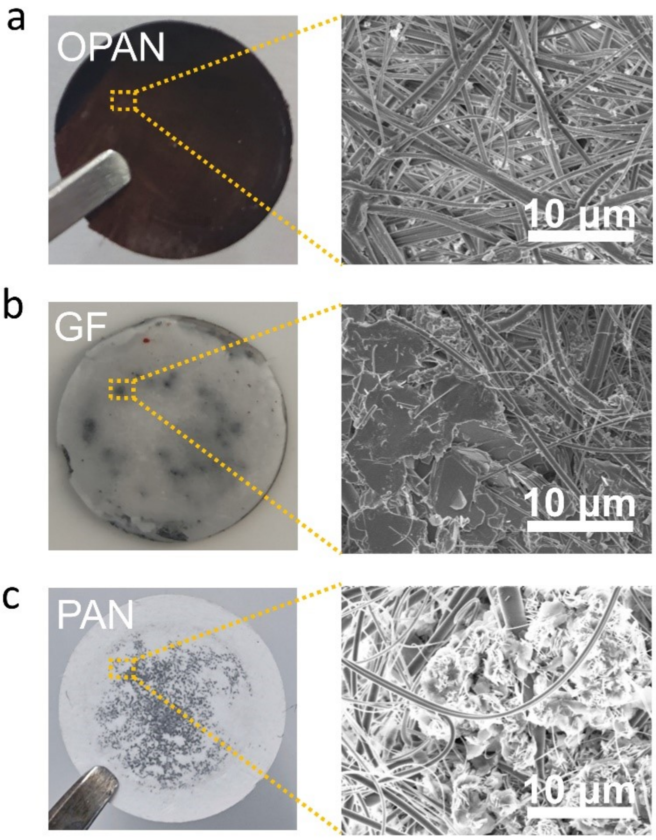

Figure S14 Optical photograph and SEM of (a) OPAN separator, (b) GF separator and (c) PAN separator after cycling at 10 mA·cm^{-2}, 10 mAh·cm^{-2}.

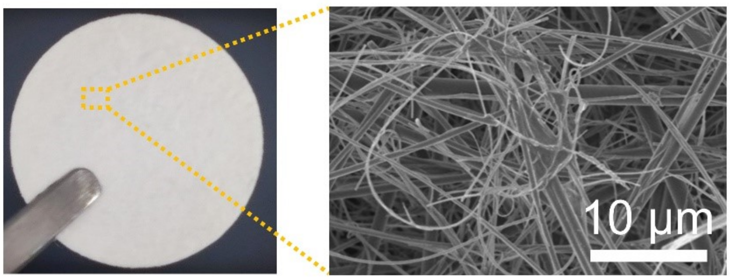

Figure S15 Optical photograph and SEM of GF separator.

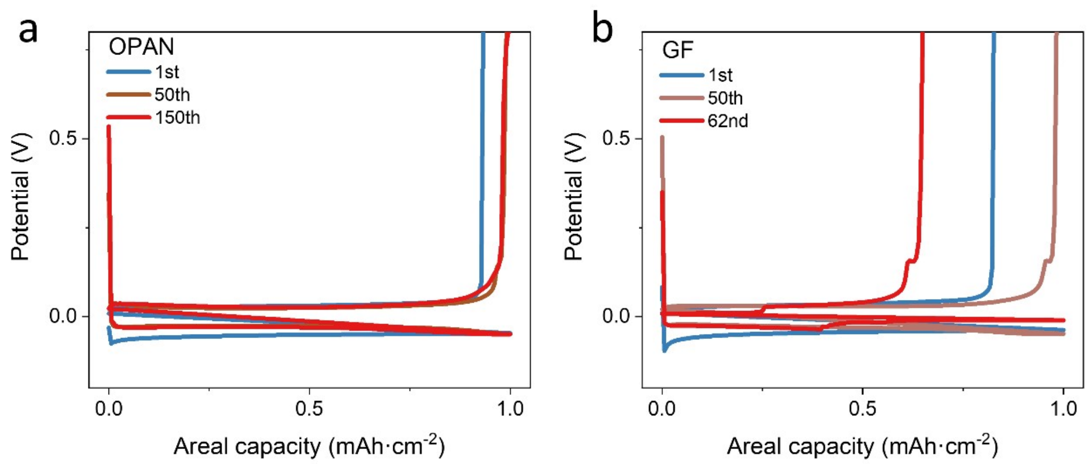

Figure S16 Voltage-capacity profiles of the Cu//Zn cell with the OPAN (a) and GF (b) separators.

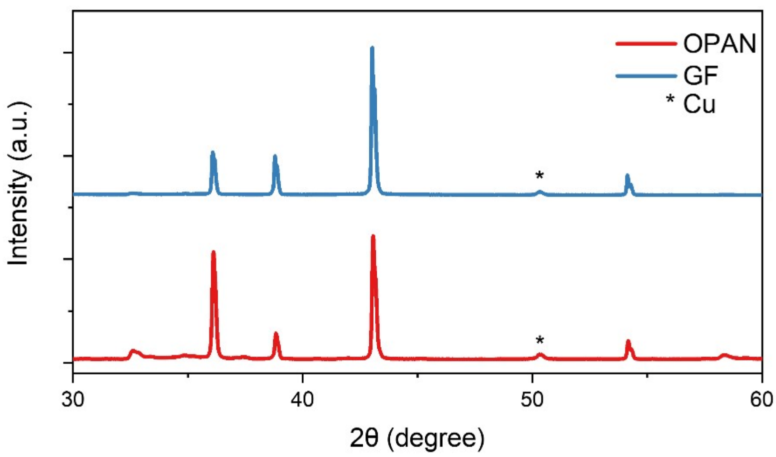

Figure S17 The XRD result of Cu current collector of Cu/OPAN/Zn and Cu/GF/Zn cells after 150 cycles.

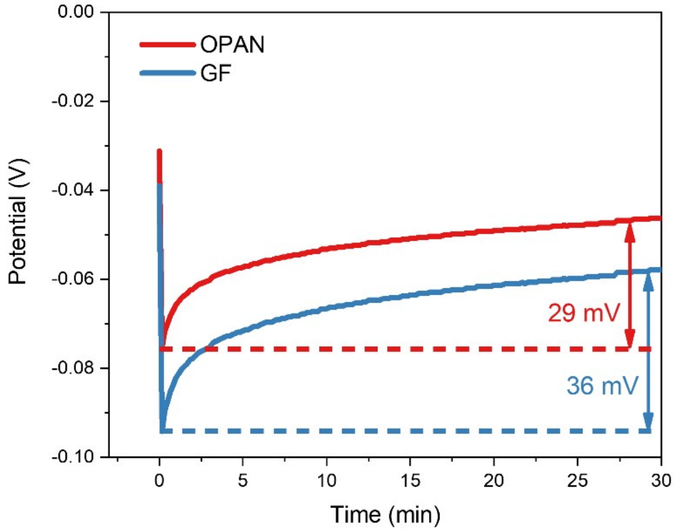

Figure S18 Voltage-time profiles of Zn//Cu cells with OPAN and GF separators.

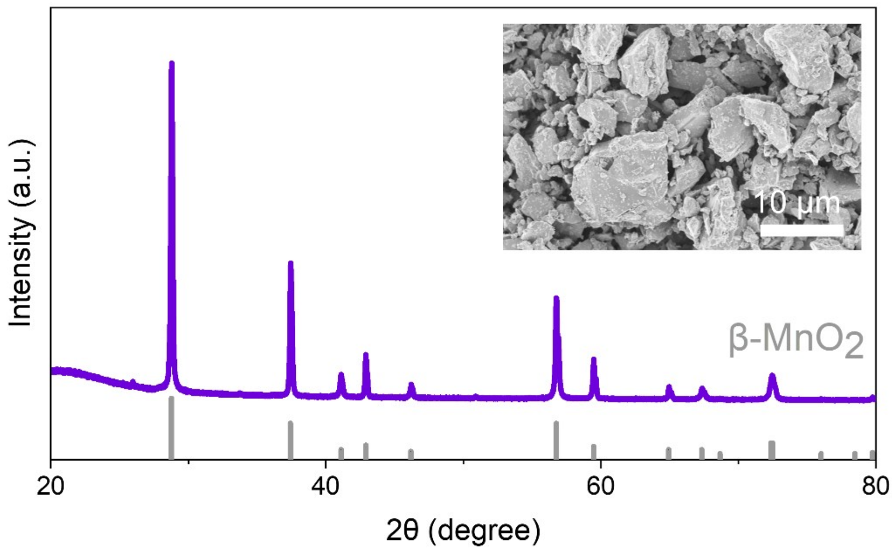

Figure S19 The XRD pattern of MnO_2 (inset is the SEM of MnO_2).

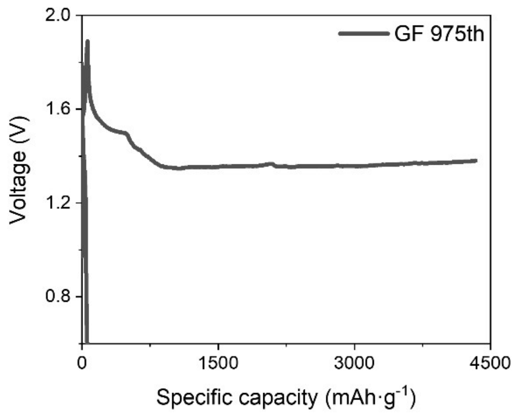

Figure S20 The Short circuit of MnO_2/GF/Zn battery at 975th cycle.

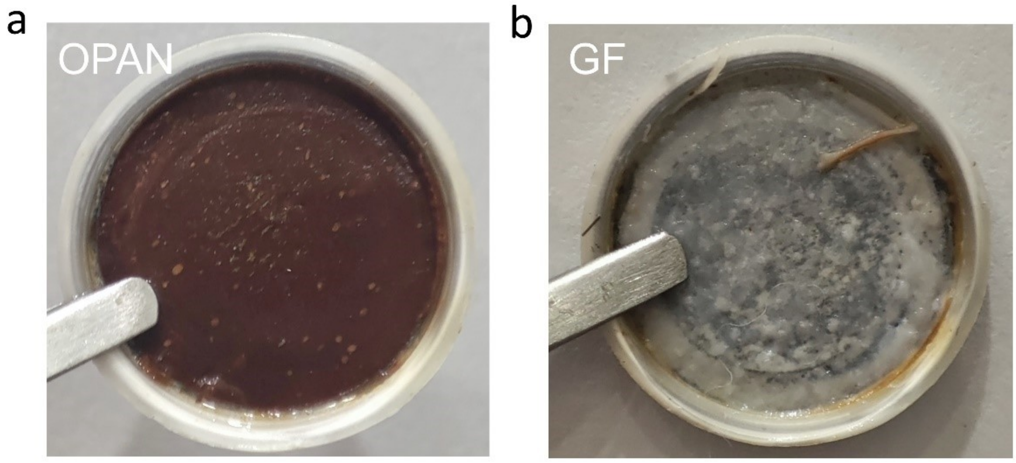

Figure S21 Optical photograph of OPAN (a) and GF (b) after the full battery durability test.

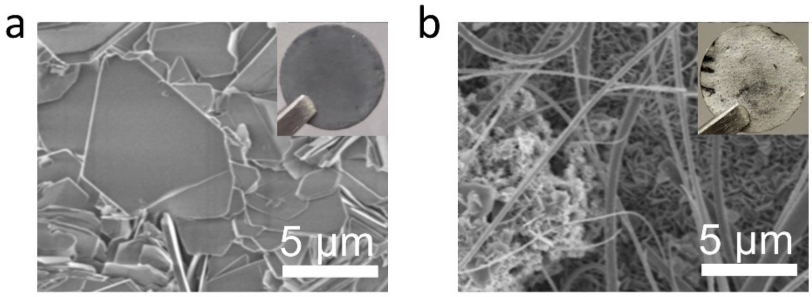

Figure S22 The SEM images and optical photograph (inset) of Zn using OPAN separator (a) and GF separator (b) after the full battery durability test.

3. Supporting Tables

Table S1 Performance comparison of Zn anodes between this work and reported studies.

Separator	Thickness (μm)	Ionic conductivity ($mS\cdot cm^{-1}$)	Zn^{2+} transference number	Lifespan of Zn//Zn cell	Reference
OPAN	100	12.6	0.955	1300 h 1 $mA\cdot cm^{-2}$ 1 $mAh\cdot cm^{-2}$	This work
PAN-S	30	3.32		350 h 0.5 $mA\cdot cm^{-2}$ 0.25 $mAh\cdot cm^{-2}$	[1]
PAN	69	4.5	0.85	800 h 0.283 $mA\cdot cm^{-2}$ 0.283 $mAh\cdot cm^{-2}$	[2]
GF@VG	200			250 h 1 $mA\cdot cm^{-2}$ 1 $mAh\cdot cm^{-2}$	[3]

GF@N-doped carbon			0.57	1100 h 1 $mA \cdot cm^{-2}$ 1 $mAh \cdot cm^{-2}$	[4]
GF@GO		13.942		500 h 2 $mA \cdot cm^{-2}$	[5]
lignin@Nafion		9.1		410 h 0.6 $mA \cdot cm^{-2}$ 0.226 $mAh \cdot cm^{-2}$	[6]
cellulose/g-C_3N_4	70	3.05	0.45	590 h 3 $mA \cdot cm^{-2}$ 1 $mAh \cdot cm^{-2}$	[7]
cellulose/GO	30	1.99		1750 h 0.5 $mA \cdot cm^{-2}$ 0.25 $mAh \cdot cm^{-2}$	[8]

Table S2 The electrochemical performance of MnO_2//Zn cells with different DOD of Zn.

Separator	Cathode mass loading	Cathode specific capacity	Corresponding weight of consumed Zn	Actual weigh of Zn (mg)	DOD/%

	(mg)	$(mAh \cdot g^{-1})$	(mg)		
OPAN	5.70	153.28	1.15	5.436	21.2
	11.50	139.83	2.12	5.308	39.9
	17.58	122.50	2.83	5.389	52.5
GF	5.66	111.49	0.83	5.395	15.4
	12.08	102.00	1.62	5.400	30.0
	17.65	93.56	2.17	5.375	40.4

Reference

[1] B.-S. Lee, S. Cui, X. Xing, H. Liu, X. Yue, V. Petrova, H.-D. Lim, R. Chen, P. Liu, Dendrite suppression membranes for rechargeable zinc batteries, ACS applied materials & interfaces 10 **45** (2018) 38928-38935.

[2] Y. Fang, X. Xie, B. Zhang, Y. Chai, B. Lu, M. Liu, J. Zhou, S. Liang, Regulating zinc deposition behaviors by the conditioner of PAN separator for zinc-ion batteries, Advanced Functional Materials 32 **14** (2022) 2109671. https://doi.org/10.1002/adfm.202109671.

[3] C. Li, Z. Sun, T. Yang, L. Yu, N. Wei, Z. Tian, J. Cai, J. Lv, Y. Shao, M. H. Rümmeli, Directly grown vertical graphene carpets as janus separators toward stabilized Zn metal anodes, Advanced Materials 32 **33** (2020) 2003425.

[4] X. Yang, W. Li, J. Lv, G. Sun, Z. Shi, Y. Su, X. Lian, Y. Shao, A. Zhi, X. Tian, In situ separator modification via CVD-derived N-doped carbon for highly reversible Zn

metal anodes, Nano Research (2021) 1-7. https://doi.org/10.1007/s12274-021-3957-z.

[5] J. Cao, D. Zhang, X. Zhang, M. Sawangphruk, J. Qin, R. Liu, A universal and facile approach to suppress dendrite formation for a Zn and Li metal anode, Journal of Materials Chemistry A 8 **18** (2020) 9331-9344. https://doi.org/10.1039/D0TA02486D.

[6] D. Yuan, W. Manalastas Jr, L. Zhang, J. J. Chan, S. Meng, Y. Chen, M. Srinivasan, Lignin@ nafion membranes forming Zn solid–electrolyte interfaces enhance the cycle life for rechargeable zinc-ion batteries, ChemSusChem 12 **21** (2019) 4889-4900. https://doi.org/10.1002/cssc.201901409.

[7] Y. Yang, T. Chen, B. Yu, M. Zhu, F. Meng, W. Shi, M. Zhang, Z. Qi, K. Zeng, J. Xue, Manipulating Zn-ion flux by two-dimensional porous g-C3N4 nanosheets for dendrite-free zinc metal anode, Chemical Engineering Journal 433 (2022) 134077. https://doi.org/10.1016/j.cej.2021.134077.

[8] J. Cao, D. Zhang, C. Gu, X. Wang, S. Wang, X. Zhang, J. Qin, Z. S. Wu, Manipulating crystallographic orientation of zinc deposition for dendrite-free zinc ion batteries, Advanced Energy Materials 11 **29** (2021) 2101299. https://doi.org/10.1002/aenm.202101299.